THE JOURNAL OF PHYSICAL CHEMISTRY LETTERS
A JOURNAL OF THE AMERICAN CHEMICAL SOCIETY

pubs.acs.org/JPCL

Letter

One-Step Synthesis of Cationic Covalent Organic Frameworks

Syed Ibrahim Gnani Peer Mohamed, Tan Zhang, Zhen Jiang, Andrew M. Rappe,* and Siamak Nejati*

Cite This: *J. Phys. Chem. Lett.* 2022, 13, 10030−10034

Read Online

ACCESS | Metrics & More | Article Recommendations | Supporting Information

ABSTRACT: Ionic covalent organic frameworks (iCOFs) have attractive properties that make them suitable for use as ion transport materials, as energy storage media, and for metal sorption. However, the synthetic pathways to prepare iCOFs are limited. Herein, we prepare an iCOF via a single-step reaction. The synthesized materials were isolated as polycrystalline nanowires. The theoretical and experimental data reveal that the synthesized iCOFs are predominately assembled into staggered configurations. The materials exhibit an uptake capacity of 3.5 $g \cdot g^{-1}$ for iodine. The *ab initio* calculations point to the role of bromide counterions, forming I_2Br^- as stable ions within the framework.

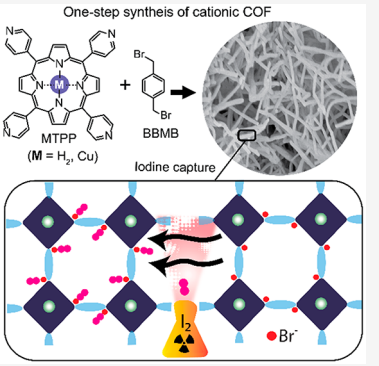

Covalent organic frameworks (COFs) have gained significant attention due to the versatility of their designs, offering opportunities to synthesize task-specific materials.[1,2] To that end, many COFs have been designed and synthesized for a variety of applications such as solid-state ion conductors and heavy-metal ion removal.[3−5] COFs carrying charged groups in their unit cells are referred to as ionic COFs (iCOFs) and have been the subject of recent interest as potential solid-state electrolyte materials in batteries.[6] The inclusion of ionic groups in COFs facilitates their use as ion conductors[7] and allows for controlling the affinity of the structure for performing selective sorption of ions.[8] Based on the sign of the charged groups on the skeletons of iCOFs, they can be classified into anionic (aCOFs) and cationic (cCOFs). The one-step synthesis of an aCOF was first achieved by the condensation of trimethyl borates and polyols.[9] Later, silicate-, imidazolate-, and sulfonate-containing aCOFs were synthesized either by using ionic monomer or through the postmodification of COFs.[10] Similarly, the synthesis of the first cCOF was reported by Ma et al.[11] where an ionic monomer was used. Following this report, a variety of cCOFs such as ethidium, guanidinium, imidazolium, and ammonium containing a cCOF were synthesized.[12]

Here, we report the synthesis of porphyrin-based cCOFs (MPOR-cCOFs, M = H_2 or Cu) via a single-step reaction, following the Menshutkin reaction.[13] Briefly, MPOR-cCOFs are synthesized by dissolving 5,10,15,20-tetra(4-pyridyl) porphyrin (TPP) or 5,10,15,20-tetra(4-pyridyl) porphyrinato copper(II) (CuTPP) along with 1,4-bis-bromomethyl-benzene (BBMB) in chloroform. The mixture is heated to reflux for 1 to 4 days under a nitrogen blanket. Then, the reaction mass is cooled to room temperature, and the precipitate is isolated by filtration, washed with chloroform, and purified with Soxhlet extraction under chloroform reflux. The dried materials are identified as MPOR-cCOF (Figure 1A). The resulting materials are positively charged in water, contain Br^- counterions, and are thermally and chemically stable. The detailed procedure for the material synthesis and characterization are given in Supporting Information, Sections S1 and S2, respectively.

Figure 1 shows the electron microscopy images of MPOR-cCOFs. We note that there are structural variations for cCOF as a function of reaction time; Figure S2 in the Supporting Information presents these structural variations. Figure 1B shows the SEM images of MPOR-cCOFs, extracted from batches with a run time of 4 days. Here the MPOR-cCOF nanofibers are the major products of the reactions. As shown in Figure 1B (i) and (iii), the average diameters of the fibers of cCOF prepared with TPP and CuTPP, referred to as POR-cCOF and CuPOR-cCOF, were found to be between 40 and 50 nm. The high-resolution transmission electron microscopy (HRTEM) images of these nanofibers are shown in Figures 1B ii, iv, and v. The lattice fringes are separated by 0.46 and 0.3 nm for POR-cCOF and CuPOR-cCOF nanofibers, respectively. Previous reports on the synthesis of cCOFs postulated a mechanism explaining the formation of cCOF nanofibers.[14,15] Here, we expect that a similar phenomenon governs the formation of these fibers. As shown in Figure 1C, the proposed

Received: August 16, 2022
Accepted: October 12, 2022
Published: October 20, 2022

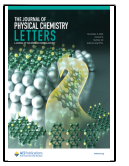

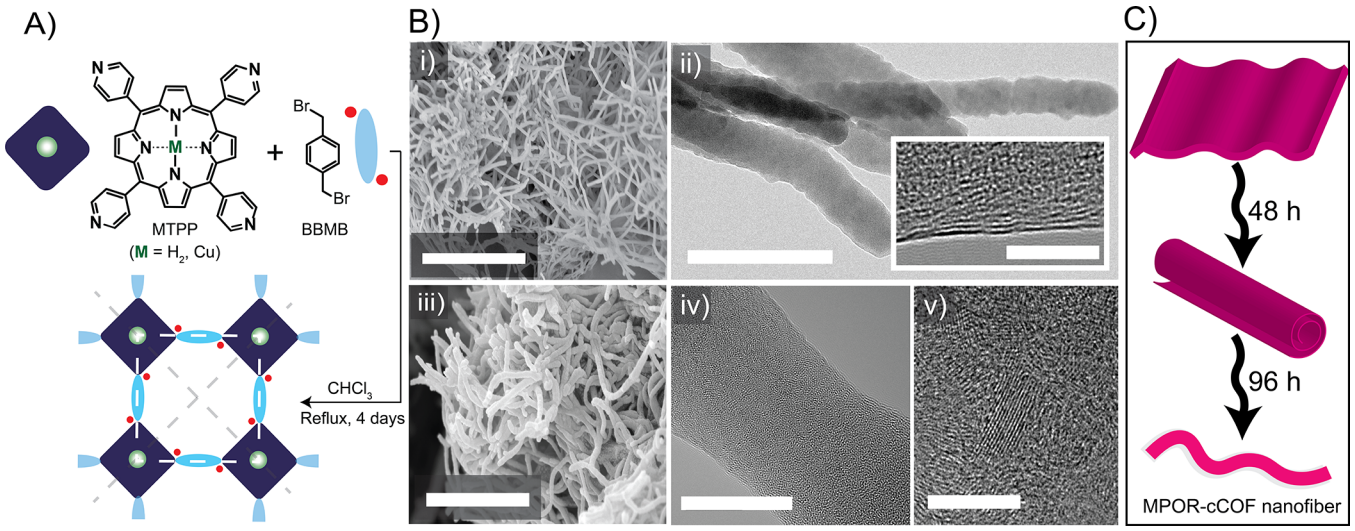

Figure 1. (A) Synthetic scheme of POR-cCOF and CuPOR-cCOF via the Menshutkin reaction. The polymerization proceeds via S_N2 reaction in refluxing chloroform to yield cCOFs. (B) Scanning and transmission electron microscopy images of synthesized cCOFs; i and ii are POR-cCOF and (iii–v) represent CuPOR-cCOF. (C) Schematic representation of the mechanism for the formation of cCOF nanofibers. Scale bars in i and iii are 1 μm, and those in ii and the inset image are 200 and 5 nm, respectively; scale bars in iv and v are 20 and 5 nm, respectively.

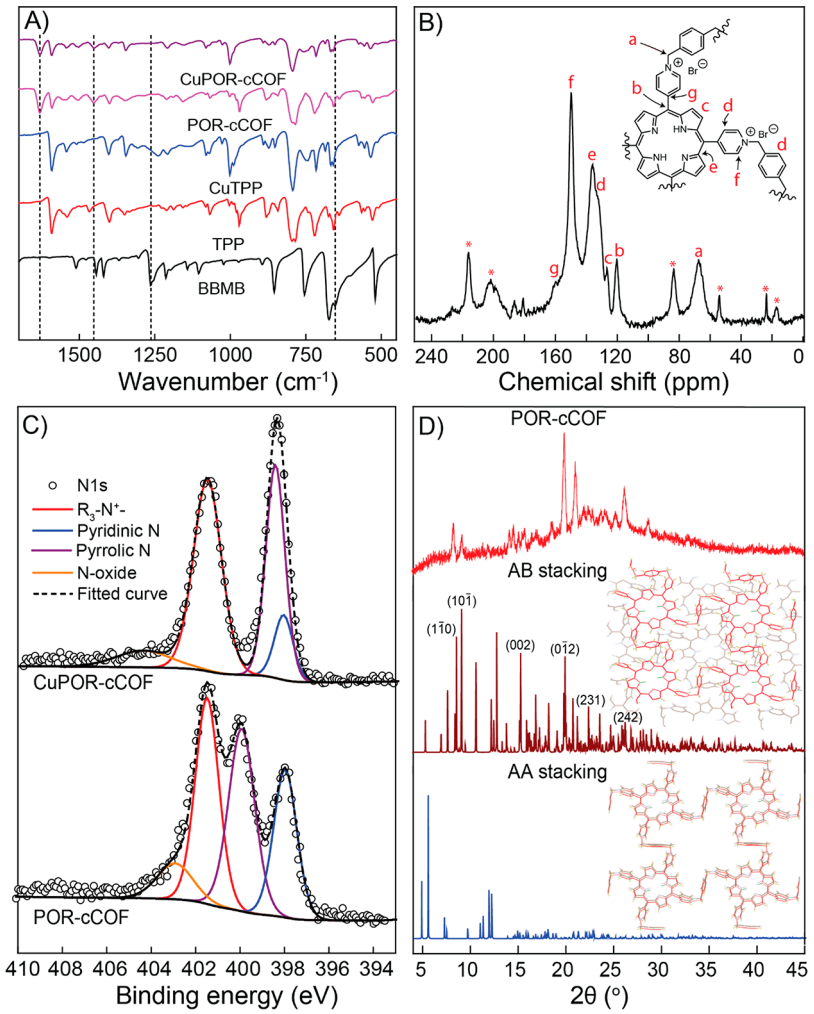

Figure 2. (A) ATR-FTIR of BBMB, TPP, CuTPP, POR-cCOF, and CuPOR-cCOF. (B) Solid-state ^{13}C CP-MAS NMR (the peaks marked with * are spinning sidebands) of POR-cCOF. (C) XPS N 1s high-resolution spectrum of POR-cCOF and CuPOR-cCOF. (D) Experimentally observed and DFT-derived PXRD pattern of POR-cCOF. The inset stick models show AA and AB stacking POR-cCOF. The color code is C (brown), N (gray), H (pink), and Br (orange).

https://doi.org/10.1021/acs.jpclett.2c02543
J. Phys. Chem. Lett. 2022, 13, 10030–10034

mechanism suggests that the crystallites of cCOFs initially agglomerate to form sheet-like aggregates that are stabilized by intermolecular forces and $\pi-\pi$ interactions.[16] As the reaction proceeds, the attractive forces between the cations and π electrons[17] induce scrolling of the sheets, forming nanofibers as thermodynamically stable structures.[18]

Fourier transform infrared spectroscopy, in attenuated total reflection mode (ATR-FTIR), was used to study the chemical structure of these cCOFs. As shown in Figure 2A, the peaks at ~1260 cm^{-1} and ~670 cm^{-1}, associated with the $-CH_2$ wagging in $-CH_2Br$ groups and the C−Br stretching,[19] are not observed in cCOFs. The absence of these vibrational bands suggests the effective reaction between BBMB and TPP, or between BBMB and CuTPP. The existence of a porphyrin moiety in cCOFs was confirmed by the presence of a vibrational peak at ~968 cm^{-1}.[20] The peak at ~1591 cm^{-1} is ascribed to the C═N vibration of pyridine moieties. This band was red-shifted to ~1631 cm^{-1} in cCOFs, suggesting the existence of a quaternary ammonium group (R_3-N^+-). The peak at ~1451 cm^{-1} in cCOFs confirms the presence of the benzylic methylene group attached to the pyridyl quaternary ammonium group.[21] These assignments were cross-examined using data from the solid-state ^{13}C cross-polarized magic-angle spinning nuclear magnetic resonance (^{13}C CP-MAS NMR) spectrum of POR-cCOF, shown in Figure 2B. The peak located at 67.3 ppm (a) confirms the presence of benzylic methylene carbon attached to the pyridyl quaternary ammonium group.[21] The peak associated with the carbons of the porphyrin ring connected to the pyridyl ring is observed at 120.2 ppm (b). The pyrrolic carbons in the porphyrin ring were found at 126.6 and 136 ppm (c and e). The carbons in benzene rings and the carbons adjoining to the pyridyl N were found at 133.1 and 149.7 ppm, (d) and (f), respectively. The resonance peak at 159.7 ppm (g) was attributed to pyridyl carbons connected to the porphyrin ring.[21]

The degree of quaternarization was further studied by X-ray photoelectron spectroscopy (XPS).[13] The XPS survey and high-resolution N 1s spectra of POR-cCOF synthesized with a reaction time of 24 h, 48 h, and 11 days are shown in Figure S3. Figure 2C shows the N 1s peak of POR-cCOF and CuPOR-cCOF, extracted from a batch with a run time of 4 days. In the case of POR-cCOF, the N 1s signal is deconvoluted into four peaks, centered at 398.4, 399.9, 401.7, and 403.1 eV, and assigned to the pyridinic N, pyrrolic N, quaternary ammonium group (R_3-N^+-),[22,23] and N-oxide, respectively. In the case of CuPOR-cCOF, shown in Figure 2C, the pyrrolic peak, due to the existence of Cu, was down-shifted by ~1 eV, and the pyridinic N, pyrrolic N, and R_3-N^+- peaks were observed at 398.2, 398.7, and 401.5 eV, respectively. We estimated the degree of quaternarization by deconvoluting the N 1s signals. The values are tabulated in Table S1 in the Supporting Information. Here, we observe an increase in quaternarization as a function of reaction time; the degree of quaternarization for POR-COF reaches values as high as 67%. In the case of CuPOR-cCOF, this value is slightly higher, reaching 78% quaternarization. We attribute this increase to the higher solubility of CuTPP. Additionally, looking at the Cu 2p XPS high-resolution spectrum, shown in Figure S5, the oxidation state of copper can be assigned as Cu^{2+}, showing that the CuPOR-cCOF porphyrin moiety remains stable.

The crystal structure of POR-cCOF was analyzed with powder X-ray diffraction (PXRD). As shown in Figure 2D, the diffractogram exhibits sharp peaks, indicating the high crystallinity of cCOFs. The corresponding 2θ values for these peaks are tabulated in the Supporting Information Section S2. To determine the cCOF crystal structures, two possible stacking configurations, staggered (AB) and eclipsed (AA) models, were proposed for two-layer cCOF repeat units. Density functional theory (DFT) calculations were performed for both models, including variable-cell relaxation, in which both the atomic coordinates and the lattice vectors are optimized. The relaxed structures are shown in the inset of Figure 2D. The lattice parameters of the AB stacking model are a = 16.7692 Å, b = 15.3640 Å, c = 13.8908 Å, α = 56.7906°, β = 94.2230°, and γ = 93.8105°. The details of the construction of the AB and AA stacking cCOFs are presented in the Supporting Information, Section S5. The stacking energy was calculated as 8.29 meV/atom and −3.78 meV/atom for the AA and AB configurations, which indicates the preference for AB stacking. The DFT-derived PXRD spectra for AA and AB configurations are shown in Figure 2D. By comparing the experimental results with the simulated diffractograms, we can assign the spectrum as showing that the AB structure is the dominant form in our samples. The simulated PXRD pattern for the AB structure features six distinct peaks at 2θ values of 8.5°, 9.1°, 15.3°, 19.9°, 21.2°, and 26.2°, which are consistent with the experimental results and correspond to the $(1\bar{1}0)$, $(10\bar{1})$, (002), $(0\bar{1}2)$, (231), and (242) facets, respectively. For CuPOR-cCOF, the experimental and theoretical PXRD patterns are shown in Figure S7.

Nitrogen sorption measurements were performed to determine the porous nature of the as-synthesized MPOR-cCOF. As shown in Figure 3A, the POR-cCOF and CuPOR-cCOF exhibit Brunauer−Emmett−Teller (BET) surface areas of 5.3 m^2/g and 15.7 m^2/g. The pore size distribution of POR-

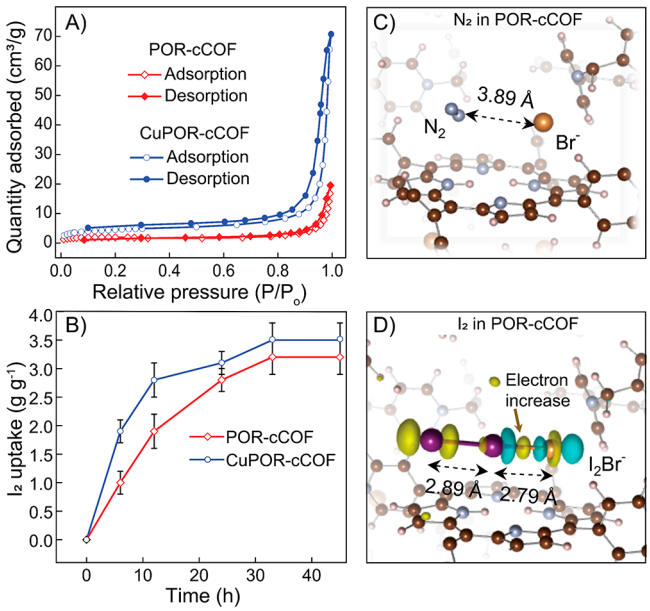

Figure 3. (A) Nitrogen sorption isotherm and (B) iodine uptake data at 75 °C and ambient pressure for POR-cCOF (red line) and CuPOR-cCOF (blue line). (C) The relaxed structure of N_2 (gray spheres) in POR-cCOF. (D) The relaxed structure of I_2 (purple spheres) in POR-cCOF. The yellow (cyan) region from electron density difference analysis shows the electron increase (decrease) during I_2 uptake.

https://doi.org/10.1021/acs.jpclett.2c02543
J. Phys. Chem. Lett. 2022, 13, 10030−10034

cCOF and CuPOR-cCOF demonstrated the presence of macroporous domains (Figure S8). Here, we attribute the small BET surface area of cCOFs to the inaccessibility of their pores, due to the presence of counteranions (Br^-).[24] In contrast, the iodine (I_2) sorption measurements, conducted at 75 °C and ambient pressure, indicated significant I_2 uptake. As shown in Figure 3B, the POR-cCOF and CuPOR-cCOF exhibited maximum I_2 uptake of ∼3.2 and 3.5 $g{\cdot}g^{-1}$. We attributed this to the presence of the ionic groups, facilitating I_2 uptake via Coulombic interactions.[25] To elucidate the contrast in the sorption capacity of cCOF toward molecular N_2 and I_2, we carry out first-principles calculations. Here, one N_2 or I_2 molecule is placed in the space between the two layers of cCOF. The relaxed structures are shown in Figure 3C and D. The result suggests that the nitrogen molecule is physisorbed within the framework, while iodine is mainly chemisorbed. The distance between N_2 and Br^- is as large as 3.89 Å, which is attributed to the high stability of N_2. By contrast, I_2 is easily chemisorbed by Br^- to form a nearly linear I_2Br^- ion. This result is consistent with the previous report.[26] The bond angle of I−I−Br is 174.9°, and the bond lengths are 2.89 and 2.79 Å for the I−I and I−Br bonds, respectively. The absorption energy of I_2 is −0.87 eV. The electron density difference map in Figure 3D shows that the electrons are accumulated (yellow region) in the newly formed I−Br chemical bond, which confirms the affinity of the synthesized cCOF toward I_2.

In summary, we report the one-step synthesis of MPOR-cCOFs nanofiber via the Menshutkin reaction using neutral starting materials and without any postmodification. The MPOR-cCOFs were found to be crystalline and chemically stable. Based on the experimental and theoretical PXRD patterns, the synthesized MPOR-cCOFs were found to be mostly composed of an AB staggered configuration. The cCOFs were effective in iodine uptake. The presence of bromide ions, forming I_2Br^- with iodine, was found to be the main reason behind the efficient iodine uptake of synthesized cCOFs. Thus, the present investigation paves the way for the one-step synthesis of iCOFs with neutral monomer and their use for iodine removal. In addition, the presence of ionic functional groups that can be exchanged makes these iCOFs more attractive for other applications such as solid-state electrolytes.

■ ASSOCIATED CONTENT

Supporting Information

The Supporting Information is available free of charge at https://pubs.acs.org/doi/10.1021/acs.jpclett.2c02543.

General procedures, experimental details of synthesis, iodine uptake, and DFT calculations. Characterizations, containing FT-IR, XRD data, SEM images, iodine uptake, XPS, and stability test. (PDF)

Transparent Peer Review report available. (PDF)

■ AUTHOR INFORMATION

Corresponding Authors

Andrew M. Rappe − *Department of Chemistry, University of Pennsylvania, Philadelphia, Pennsylvania 19104-6323, United States;* orcid.org/0000-0003-4620-6496; Email: rappe@sas.upenn.edu

Siamak Nejati − *Department of Chemical and Biomolecular Engineering, University of Nebraska—Lincoln, Lincoln, Nebraska 68588-8286, United States;* orcid.org/0000-0002-1807-2796; Email: snejati2@unl.edu

Authors

Syed Ibrahim Gnani Peer Mohamed − *Department of Chemical and Biomolecular Engineering, University of Nebraska—Lincoln, Lincoln, Nebraska 68588-8286, United States;* orcid.org/0000-0001-9460-8620

Tan Zhang − *Department of Chemistry, University of Pennsylvania, Philadelphia, Pennsylvania 19104-6323, United States*

Zhen Jiang − *Department of Chemistry, University of Pennsylvania, Philadelphia, Pennsylvania 19104-6323, United States;* orcid.org/0000-0002-1175-5658

Complete contact information is available at: https://pubs.acs.org/10.1021/acs.jpclett.2c02543

Notes

The authors declare no competing financial interest.

■ ACKNOWLEDGMENTS

The experimental work was supported in part by the National Science Foundation, under Grant Number CBET-2047291. The theoretical study by Z.J. and A.M.R. of the chemical reactivity of iCOFs was supported by the U.S. Department of Energy, Office of Science, Office of Basic Energy Sciences, under Grant Number DE-SC0019281. Theoretical studies by T.Z. and A.M.R. of the atomic and electronic structure of iCOFs were supported by the National Science Foundation, under Grant Number DMR-1720530. Computational support was provided by the National Energy Research Scientific Computing Center (NERSC), a U.S. Department of Energy, Office of Science User Facility located at Lawrence Berkeley National Laboratory, operated under Contract No. DE-AC02-05CH11231. The characterizations were performed in part in the Nebraska Nanoscale Facility: National Nanotechnology Coordinated Infrastructure and the Nebraska Center for Materials and Nanoscience, which are supported by the National Science Foundation under Award ECCS: 1542182, and the Nebraska Research Initiative.

■ REFERENCES

(1) Cote, A. P.; Benin, A. I.; Ockwig, N. W.; O'Keeffe, M.; Matzger, A. J.; Yaghi, O. M. Porous, Crystalline, Covalent Organic Frameworks. *science* **2005**, *310* (5751), 1166−1170.

(2) Diercks, C. S.; Yaghi, O. M. The Atom, the Molecule, and the Covalent Organic Framework. *Science* **2017**, *355* (6328), eaal1585.

(3) Tang, C.; Qin, Y.; Ni, C.; Zou, J. Detection and Removal of Mercury Ions in Water by a Covalent Organic Framework Rich in Sulfur and Nitrogen. *ACS Appl. Polym. Mater.* **2022**, *4* (2), 849−858.

(4) Li, X.; Loh, K. P. Recent Progress in Covalent Organic Frameworks as Solid-State Ion Conductors. *ACS Mater. Lett.* **2019**, *1* (3), 327−335.

(5) Lu, Y.; Cai, Y.; Zhang, Q.; Chen, J. Structure−Performance Relationships of Covalent Organic Framework Electrode Materials in Metal-Ion Batteries. *J. Phys. Chem. Lett.* **2021**, *12* (33), 8061−8071.

(6) Liang, X.; Tian, Y.; Yuan, Y.; Kim, Y. Ionic Covalent Organic Frameworks for Energy Devices. *Adv. Mater.* **2021**, *33* (52), 2105647.

(7) Du, Y.; Yang, H.; Whiteley, J. M.; Wan, S.; Jin, Y.; Lee, S.; Zhang, W. Ionic Covalent Organic Frameworks with Spiroborate Linkage. *Angew. Chem., Int. Ed.* **2016**, *55* (5), 1737−1741.

(8) Xiao, Y.; Ma, C.; Jin, Z.; Wang, J.; He, L.; Mu, X.; Song, L.; Hu, Y. Functional Covalent Organic Framework for Exceptional Fe2+, Co2+ and Ni2+ Removal: An Upcycling Strategy to Achieve Water

Decontamination and Reutilization as Smoke Suppressant and Flame Retardant Simultaneously. *Chem. Eng. J.* **2021**, *421*, 127837.
(9) Du, Y.; Yang, H.; Whiteley, J. M.; Wan, S.; Jin, Y.; Lee, S.; Zhang, W. Ionic Covalent Organic Frameworks with Spiroborate Linkage. *Angew. Chem., Int. Ed.* **2016**, *55* (5), 1737−1741.
(10) Liang, X.; Tian, Y.; Yuan, Y.; Kim, Y. Ionic Covalent Organic Frameworks for Energy Devices. *Adv. Mater.* **2021**, *33* (52), 2105647.
(11) Ma, H.; Liu, B.; Li, B.; Zhang, L.; Li, Y.-G.; Tan, H.-Q.; Zang, H.-Y.; Zhu, G. Cationic Covalent Organic Frameworks: A Simple Platform of Anionic Exchange for Porosity Tuning and Proton Conduction. *J. Am. Chem. Soc.* **2016**, *138* (18), 5897−5903.
(12) Zhang, P.; Wang, Z.; Cheng, P.; Chen, Y.; Zhang, Z. Design and Application of Ionic Covalent Organic Frameworks. *Coord. Chem. Rev.* **2021**, *438*, 213873.
(13) Joo, M.; Shin, J.; Kim, J.; You, J. B.; Yoo, Y.; Kwak, M. J.; Oh, M. S.; Im, S. G. One-Step Synthesis of Cross-Linked Ionic Polymer Thin Films in Vapor Phase and Its Application to an Oil/Water Separation Membrane. *J. Am. Chem. Soc.* **2017**, *139* (6), 2329−2337.
(14) Dey, K.; Mohata, S.; Banerjee, R. Covalent Organic Frameworks and Supramolecular Nano-Synthesis. *ACS Nano* **2021**, *15* (8), 12723−12740.
(15) Zhang, Z.; Shi, X.; Wang, R.; Xiao, A.; Wang, Y. Ultra-Permeable Polyamide Membranes Harvested by Covalent Organic Framework Nanofiber Scaffolds: A Two-in-One Strategy. *Chem. Sci.* **2019**, *10* (39), 9077−9083.
(16) Sun, W.; Wang, H.; Qi, D.; Wang, L.; Wang, K.; Kan, J.; Li, W.; Chen, Y.; Jiang, J. 5, 10, 15, 20-Tetra (4-Pyridyl) Porphyrinato Zinc Coordination Polymeric Particles with Different Shapes and Luminescent Properties. *CrystEngComm* **2012**, *14* (22), 7780−7786.
(17) Kennedy, C. R.; Lin, S.; Jacobsen, E. N. The Cation−π Interaction in Small-molecule Catalysis. *Angew. Chem., Int. Ed.* **2016**, *55* (41), 12596−12624.
(18) Huang, W.; Jiang, Y.; Li, X.; Li, X.; Wang, J.; Wu, Q.; Liu, X. Solvothermal Synthesis of Microporous, Crystalline Covalent Organic Framework Nanofibers and Their Colorimetric Nanohybrid Structures. *ACS Appl. Mater. Interfaces* **2013**, *5* (18), 8845−8849.
(19) Silverstein, R. M.; Bassler, G. C. Spectrometric Identification of Organic Compounds. *J. Chem. Educ.* **1962**, *39* (11), 546.
(20) Walter, M. G.; Wamser, C. C. Synthesis and Characterization of Electropolymerized Nanostructured Aminophenylporphyrin Films. *J. Phys. Chem. C* **2010**, *114* (17), 7563−7574.
(21) Jayakumar, S.; Li, H.; Chen, J.; Yang, Q. Cationic Zn−Porphyrin Polymer Coated onto CNTs as a Cooperative Catalyst for the Synthesis of Cyclic Carbonates. *ACS Appl. Mater. Interfaces* **2018**, *10* (3), 2546−2555.
(22) Ibrahim, G. P. S.; Isloor, A. M.; Inamuddin; Asiri, A. M.; Ismail, N.; Ismail, A. F.; Ashraf, G. M. Novel, One-Step Synthesis of Zwitterionic Polymer Nanoparticles via Distillation-Precipitation Polymerization and Its Application for Dye Removal Membrane. *Sci. Rep.* **2017**, *7* (1), 15889.
(23) Ibrahim, G. P.S; Isloor, A. M.; Bavarian, M.; Nejati, S. Integration of Zwitterionic Polymer Nanoparticles in Interfacial Polymerization for Ion Separation. *ACS Appl. Polym. Mater.* **2020**, *2* (4), 1508−1517.
(24) Jansone-Popova, S.; Moinel, A.; Schott, J. A.; Mahurin, S. M.; Popovs, I.; Veith, G. M.; Moyer, B. A. Guanidinium-Based Ionic Covalent Organic Framework for Rapid and Selective Removal of Toxic Cr (VI) Oxoanions from Water. *Environ. Sci. Technol.* **2019**, *53* (2), 878−883.
(25) Xie, Y.; Pan, T.; Lei, Q.; Chen, C.; Dong, X.; Yuan, Y.; Shen, J.; Cai, Y.; Zhou, C.; Pinnau, I.; Han, Y. Ionic Functionalization of Multivariate Covalent Organic Frameworks to Achieve an Exceptionally High Iodine-Capture Capacity. *Angew. Chem., Int. Ed.* **2021**, *60* (41), 22432−22440.
(26) Babu, R.; Bhargavi, G.; Rajasekharan, M. Synthesis, Crystal Structures, Raman and EPR Studies of Mixed Trihalides in Association with Transition Metal (CoII−ZnII) Tris-Chelates. *J. Chem. Crystallogr.* **2017**, *47* (3), 86−94.

https://doi.org/10.1021/acs.jpclett.2c02543
J. Phys. Chem. Lett. 2022, 13, 10030−10034